Available online at www.sciencedirect.com
ScienceDirect
Sensors and Actuators A 145–146 (2008) 116–122
SENSORS AND ACTUATORS A PHYSICAL
www.elsevier.com/locate/sna

A hybrid-assembled MEMS Fabry-Pérot wavelength tunable filter

Toshio Yamanoi [a,b,*], Takashi Endo [b,1], Hiroshi Toshiyoshi [c,2]

[a] *Yamaichi Electronics Co., Ltd., Ohta-ku, Tokyo, Japan*
[b] *Koshin Kogaku Co., Ltd., Hadano, Kanagawa, Japan*
[c] *Institute of Industrial Science, The University of Tokyo, Tokyo, Japan*

Received 30 June 2007; received in revised form 29 September 2007; accepted 19 October 2007
Available online 20 February 2008

Abstract

We have developed a wavelength tunable fiber optic filter by using a hybrid-assembly technique of glass reflector cubes (volume 1 mm^3) onto a bulk-micromachined electrostatic translation stage (4 mm × 5 mm). More than 0.6-μm-change of the Fabry-Pérot interferometer gap could be electrostatically controlled with a tuning voltage upwards of 4 V with the aid of a DC bias voltage of 64 V. A wide tuning range from 1479 to 1590 nm was achieved with a bandwidth of 1.3–1.2 nm and insertion loss of 1.59–1.76 dB.

Keywords: Fabry-Pérot interferometer; Wavelength tunable filter; Optical MEMS; Fiber optics

1. Introduction

Wavelength filter is an indispensable component for optical analyzing instruments and for the wavelength-division multiplexing (WDM) optical fiber network [1]. Optical signals of particular wavelengths are added to or dropped from the optical fiber network, by which the network would re-configure itself according to the traffic demands. MEMS (microelectromechanical system) approach is beneficial to make compact wavelength tunable filters thanks to the batch-processing capability, compared with the conventional technology based upon precision machining. MEMS type wavelength filters and tunable lasers have been reported [1–10], in which the air gap of the Fabry-Pérot interferometer [11] is mechanically tuned to change the resonating wavelength. Thanks to the scale of optical wavelength, micromechanical displacement in the sub-micron to micron range would suffice to tune the filter characteristics. Most MEMS version of Fabry-Pérot reflectors were made by, for instance, using multiple layers of thin films deposition on or etched in a silicon micromechanism. Due to the process restriction such as the residual stress, however, optical performance of such filters would sometimes be compromised, compared with those made on an optical-grade glass substrate. It was also reported that the Fabry-Pérot interferometer of small mass suffered from mechanical disturbance associated to the pressure of light [12]. For better optical performance, we have newly developed a post-processing technique to mount a pair of glass reflector cubes onto a MEMS actuator platform to compose a wavelength tunable filter.

2. Hybrid-assembled optical filter

Fig. 1 illustrates the device structure, in which reflector cubes are mounted on a microplatform with the high-reflection (HR) surfaces inside the gap, having the anti-reflection (AR) surfaces outside. Incident and transmitted light beams are coupled with a pair of collimator-equipped single mode fibers placed normal to the AR-surfaces of the reflector cubes. The actuator stage is designed to increase the Fabry-Pérot gap between the cubes in a micron scale and to make an electromechanically tunable Fabry-Pérot interferometer; therefore, transmission peak wavelength shifts toward longer wavelengths with increasing drive voltage. MEMS tunable filters made of multiple thin films deposited on microstructure have been reported [6,9] but the optical performance could be influenced by the mechanical deformation of the filter plates due to the residual stress of the

* Corresponding author. Tel.: +81 3 3778 6124.
E-mail addresses: yamanoi@yamaichi.co.jp (T. Yamanoi), t-endo@koshin-kogaku.co.jp (T. Endo), hiro@iis.u-tokyo.ac.jp (H. Toshiyoshi).
[1] Tel.: +81 463 74 1550.
[2] Tel.: +81 3 5452 6276.

0924-4247/$ – see front matter
doi:10.1016/j.sna.2007.10.080

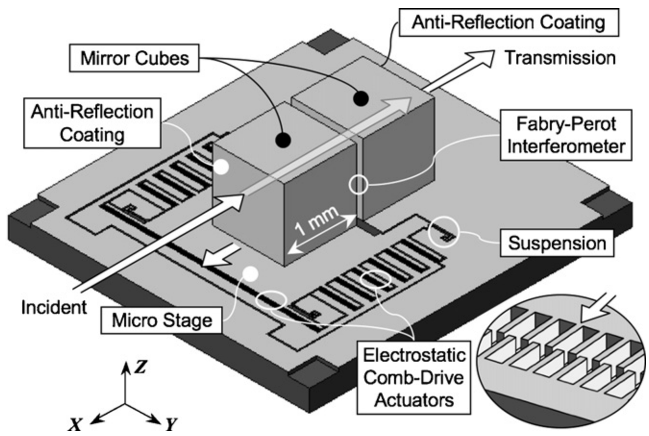

Fig. 1. Hybrid-assembled wavelength tunable filter.

films. Technical difficulty also lies in process compatibility with sacrificial release in hydrofluoric acid. On the contrary, our approach uses optical reflector that has been already made on a glass cube; reflector cubes of appropriate optimal performance can be chosen from the shelves.

As shown in the scanning electron microscope (SEM) image in Fig. 2(a), the MEMS platform actuator had a stage suspended with a four pair of straight beams on a silicon chip of 4 mm × 6 mm. The stage was 1.8 mm × 1.5 mm in area, such that it could hold one of the reflector cubes of 1 mm × 1 mm in footprint. Fig. 2(b) shows a part of the electrostatic mechanism (shown by the square in Fig. 2(a)). The electrostatic comb-drive mechanism was chosen rather than the parallel-plates actuators for its long travel range before electrostatic pull-in. The suspension was 4 μm in width, 250 μm in length, and 50 μm in height. The comb-drive fingers were designed to be 5 μm in width, 30 μm in length, and with a gap of 1.5 μm. Total of more than 648 pairs of comb-drive fingers were arranged on the stage for electrostatic operation and on the side ribs. The supporting part of the suspension root was designed to be folded to accommodate the stress of thermal deformation of the substrate chip and that from the glue used to fix the reflector cubes.

3. Fabrication process and results

Fig. 3 shows the simplified fabrication process steps based on the silicon bulk-micromachining. A silicon-on-insulator (SOI) wafer of a 50-μm-thick single crystalline silicon, a 3-μm-thick buried oxide (BOX), and a 300-μm-thick handle wafer was processed by the deep reactive-ion etching (DRIE) on the both surfaces. A photoresist Shipley S-1818 spun at 3000 rpm was used for the front-side DRIE, and a 100-nm-thick evaporated aluminum layer was used as an etching mask for the backside DRIE.

After releasing the mechanical parts by selectively removing the buried oxide in a hydrofluoric acid, a pair of glass reflector cube (1 mm^3 each) was placed with a chip-bonding tool and fixed with UV-epoxy dispensed on the foot of the reflectors. A special care was paid to keep the cube surfaces to be in parallel for a narrow bandwidth of the wavelength filtering characteristics. At this initial status, the reflector cubes were placed in contact to each other, and they were separated later by using the built-in microactuator. Techniques to mount an optical component on MEMS have been known long [13–16]. To our best knowledge, this is the first report on mounting two optical components with fairly good parallelism. Statistical analysis of assembly results is under investigation and it will be reported elsewhere.

The device after reflector-cube assembly was wire-bonded for electrical interconnection as shown in Fig. 4. Despite the relatively large mass of the cubes compared with that of the microplatform, no serious deformation of the movable stage was observed. The weight of the 1 mm cube glass (density 2.65 g/cm^3) is estimated to be 2.65 mg (or 2.6 kg m/s^2 in gravity). The surface-normal rigidity of the four pairs of suspension is, on the other hand, written as $k_v = 4 \times E(wh^3/l^3)$, where E is the Young's modulus of silicon (160 GPa), w is the suspension width (4 μm), h is the suspension height (SOI thickness, 50 μm), and l is the length (250 μm). Using these dimensions, the spring constant is calculated to be $k_v = 2.05 \times 10^4$ N/m, and the vertical deflection of the stage due to the glass cube is estimated to be 1 nm, which could be negligible to the electrostatic performance of the actuator.

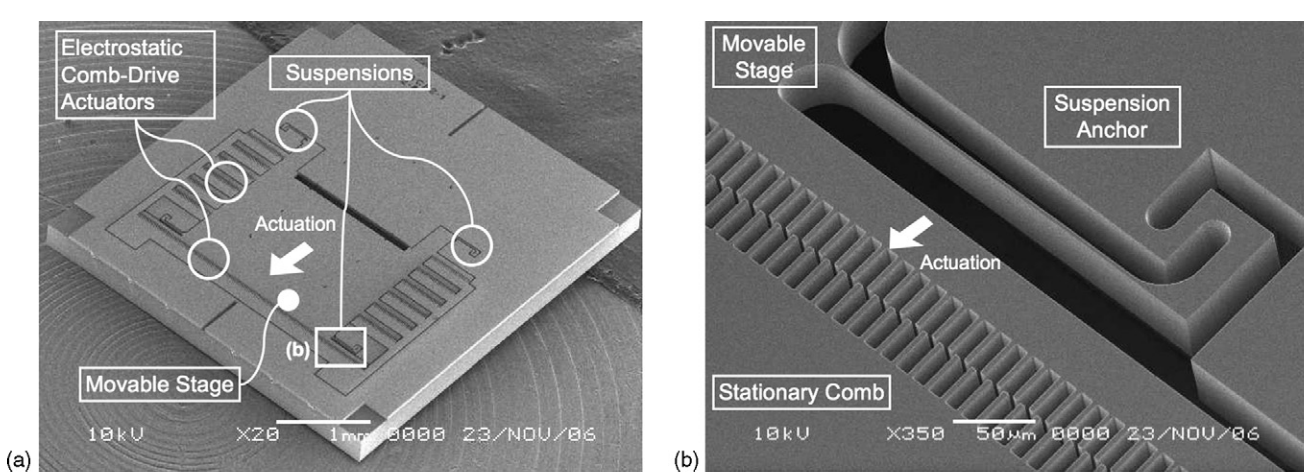

Fig. 2. SEM images of stage microactuator before reflector-cube assembly: (a) entire view and (b) a close-up view of the suspension and comb-drive electrodes.

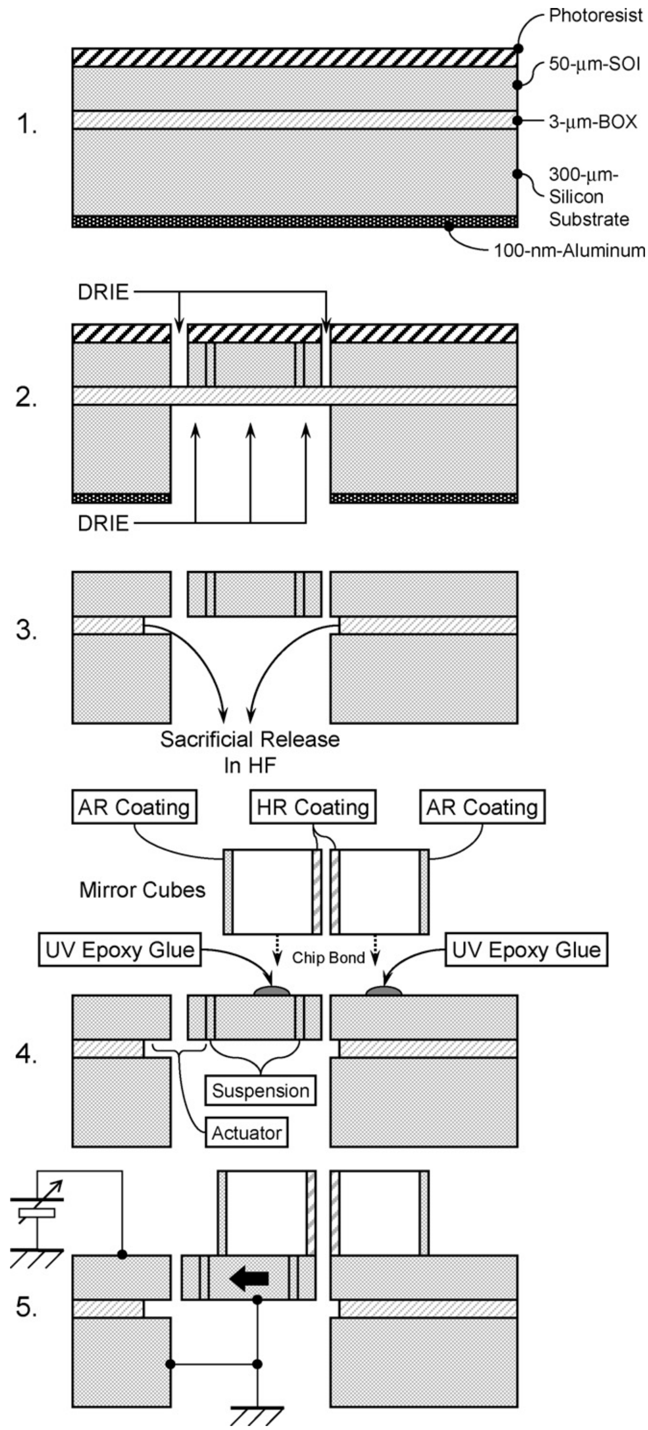

Fig. 3. Fabrication process steps for making bulk-micromachined tuning stage and hybrid-assembly of reflector cubes.

4. Characterization

4.1. Electromechanical performance of platform stage

To make the parallelism of the air gap, the cubes were put together when mounted on the stage, and the electrostatic actuator was used to pull one of them to make the Fabry-Pérot gap. The gap was observed in the SEM to see the open and close operation of the electrostatic force. Fig. 5(a) shows the close-up image of the cube interface, which was completely closed at 0 V. On the contrary, a gap could be seen at a drive voltage of 70 V in Fig. 5(b). Mechanical stopper was installed in the mechanism to avoid electrical short circuits between the comb-drive electrodes.

Circles in Fig. 6 plot a typical stage-displacement (with a glass cube mounted) as a function of net voltage applied to the actuator's electrodes. The stage-displacement with respect to the initial position was measured by the scanning laser microscope (Lasertec Corp., Japan, model 1LM15, equipped with the dimension measurement scale) as a function of applied voltage. The displacement curve could be explained well with the theoretical fitting curve of the comb-drive mechanism (solid curve); a total analytical model including the Fabry-Pérot optics is presented in Section 5. Measurement was carried out in the moisture-controlled cleanroom environment. We had anticipated the influence of the adhesion force between the mirror surfaces but the electrostatic microactuator was found to overcome it. Laser Doppler observation (Neoark Corp., Japan, model MLD-103) discovered that the stage had the pitch motion around the *X*-axis (show in Fig. 1) superposed upon the lateral motion along the *Y*-axis, thanks to the actuator force acting on the bottom surface of the cube. Hence, the mechanism was understood that the actuator gave a torque to the mirror and it effectively separated the surfaces from the bottom.

We have developed nearly 100 pieces of such Fabry-Pérot MEMS devices, and Fig. 6 shows the most successful results. Some devices were found to have irregular behavior in the displacement–voltage curve, as shown in Fig. 7, where the MEMS stage remained still until a large bias voltage (∼50 V) was applied. After the gap opening, the actuator exhibited linear motion with respect to the voltage in a range from 50 to 70 V. Nevertheless, the displacement disappeared before the voltage was set to zero. Such irregular motion was plausibly caused by the initial position offset of the reflector cube mounted on the stage. The stage could have been displaced toward the comb-drive electrodes (to the left-hand side in Fig. 4) by the lateral positioning error of the die bonder, and the mirror was glued at the position. Thus, the initial offset was given to the stage, by

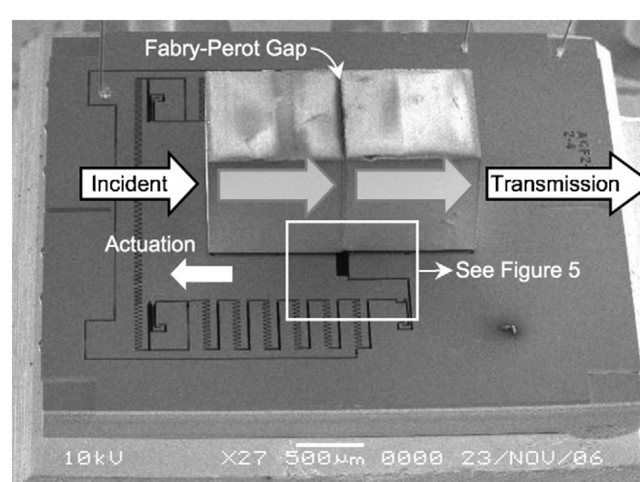

Fig. 4. SEM image of wavelength tunable filter after reflector-cube assembly.

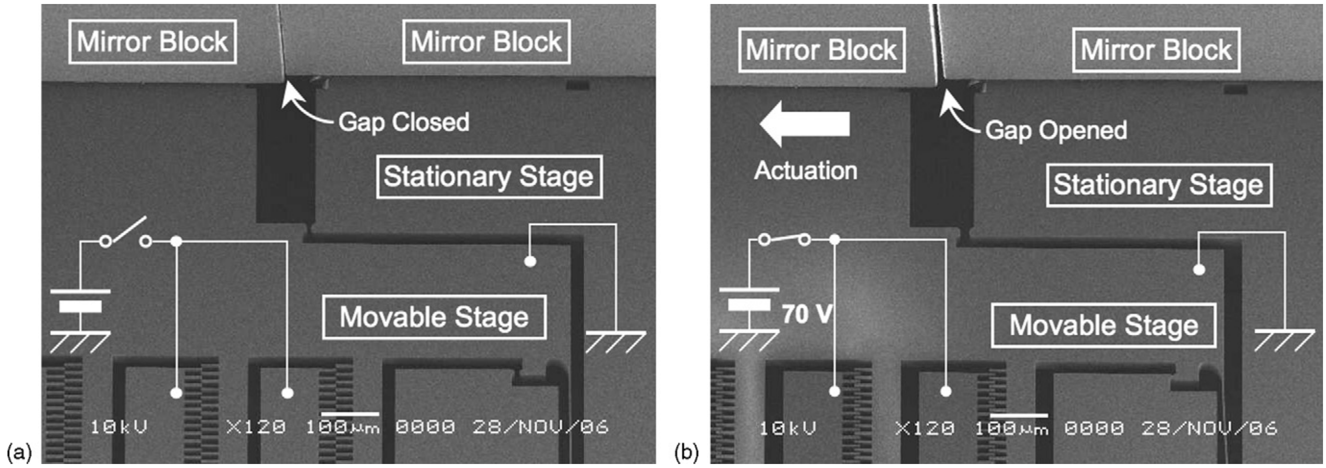

Fig. 5. Wavelength tunable filter in electrostatic operation. (a) Gap closed without operation voltage and (b) gap opened with drive voltage 70 V.

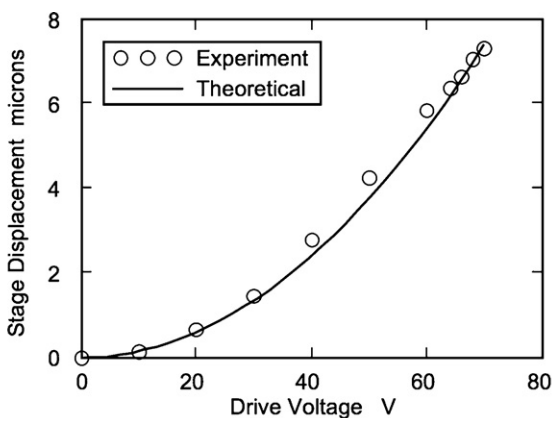

Fig. 6. Hysteresis curve of displacement as a function of drive voltage.

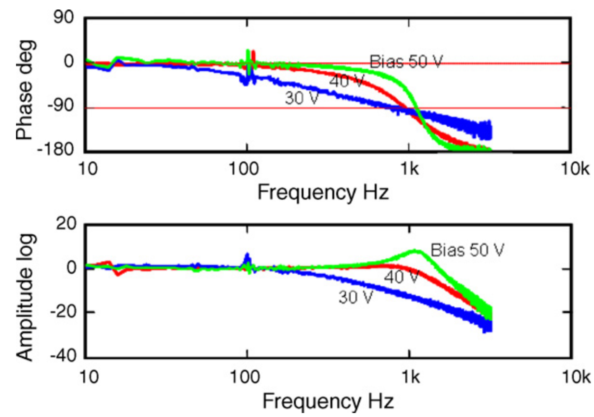

Fig. 8. Frequency response curves of electrostatically actuated reflector cube, measured at different bias voltages.

which the movable reflector cube was pushed onto the fixed one, leading to large voltage to start opening the gap. This assembly manipulation was intentionally performed to have the Fabry-Pérot gap closed at the initial states. However, finished device of excess drive voltage was ruled out before final assembly with optical fibers and a metal package. Assembly process utilizing optical monitoring is under development to improve the production yield.

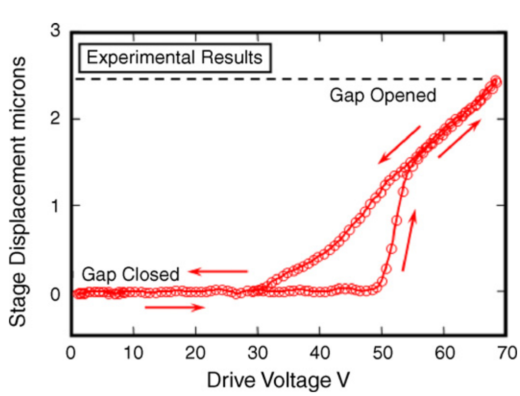

Fig. 7. Stage-displacement–voltage curve that was influenced by the initial position offset of the reflector cubes.

Frequency responses of the stage oscillation at different bias voltages were observed after gap opening. Mechanical resonant peak with a reflector cube on was observed at 1 kHz only when the average gap opening was large, as shown in Fig. 8. At lower voltages, the air viscosity became dominant due to the small Fabry-Pérot gap, and hence the stage oscillation was over-damped.

4.2. Wavelength tuning performance

In Fig. 9(a), we show the optical apparatus to measure the reflectivity of the mirror cube in between a pair of single mode fiber with collimators. Transmission spectra were measured with and without the reflector cube, by using a light source (FiberLab Inc., ASE-FL7701) and an optical signal analyzer (Agilent, 86140B) and were converted into the reflection as shown in Fig. 10. More than 98% reflectivity was obtained within the wavelength of interest (1480–1590 nm).

We placed the developed MEMS filter in between the pair of collimators, as illustrated in Fig. 9(b), and plot the shift of the peak wavelength by observing the transmission spectrum. Thanks to the high reflectivity of the reflector cube over the

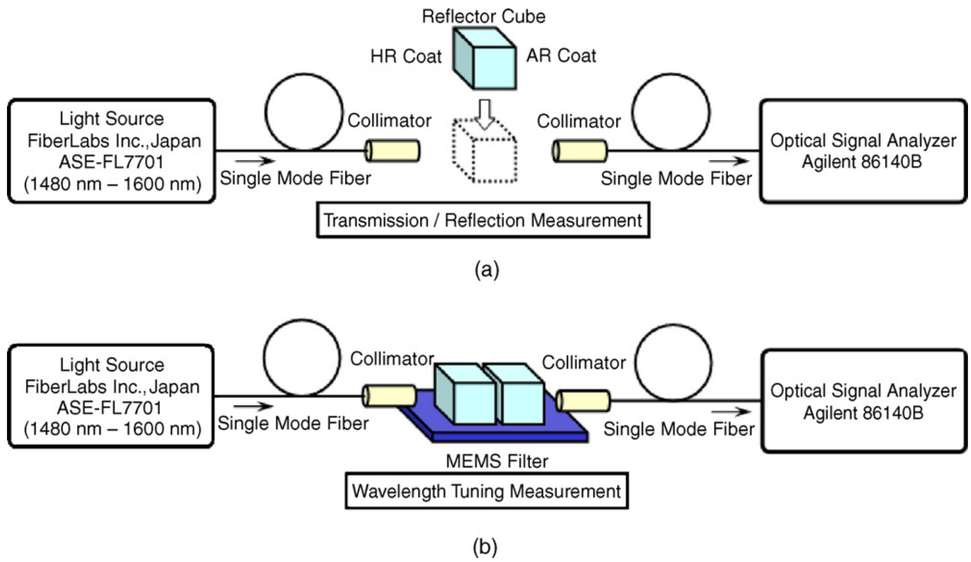

Fig. 9. Optical apparatus for characterization. (a) Reflectivity measurement of the mirror cube and (b) wavelength tuning measurement of the developed MEMS Fabry-Pérot filter.

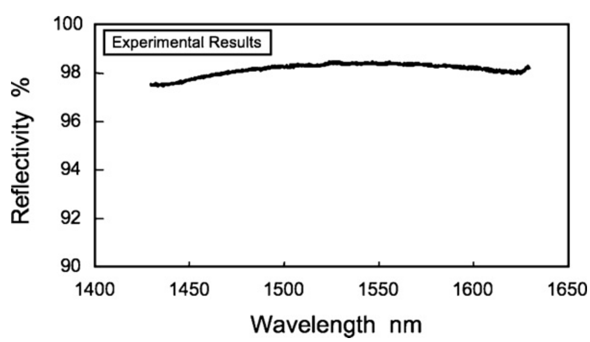

Fig. 10. Wavelength characteristics of reflector cube.

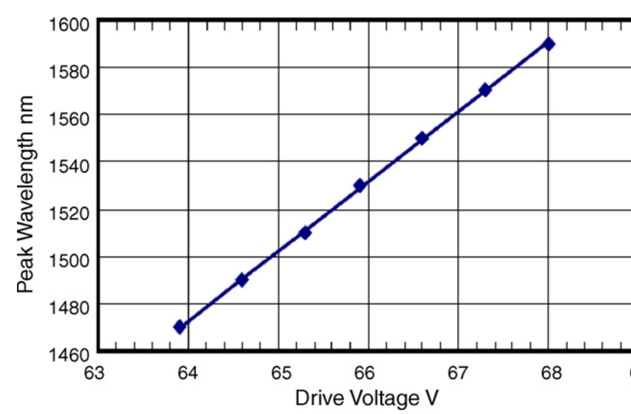

Fig. 12. Transmission peak as a function of applied voltage.

wide wavelength range and also to the low loss of the glass cube, the spectrum was found to have a narrow bandwidth (FWHM 1.2–1.3 nm). We used the voltage range of 63.9–68 V to control the transmission peak wavelength shifted from 1479 to 1590 nm, as shown in Fig. 11. This covers a wide tuning range over 110 nm. Also thanks to the linearity of comb-drive electrostatic actuation, the peak shift was found to be fairly linear with respect to the applied voltage, as shown in Fig. 12. Insertion loss was small (1.59–1.76 dB) and it was found to be sensitive to the mirror deviation from parallel gap. Therefore, the reflector cubes were not mounted one-by-one but they were put together when mounted on the MEMS chip. Optical performance of the wavelength tuning is summarized in Table 1.

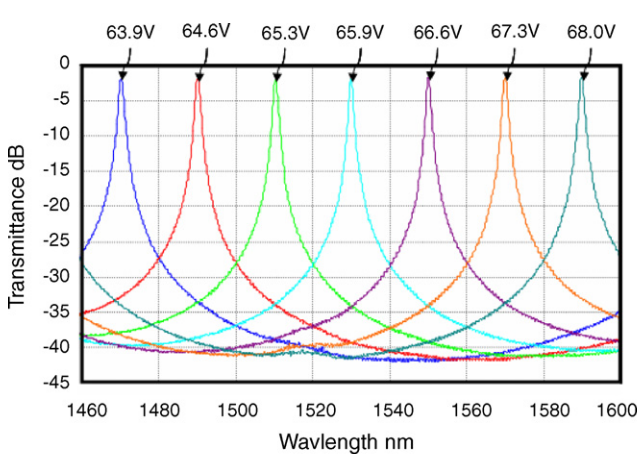

Fig. 11. Transmission wavelength spectrum of the MEMS Fabry-Pérot filter.

Table 1
Summary of wavelength tuning performance

Drive voltage	63.9 V	68.0 V
Fabry-Pérot Gap	6.4 μm	7.0 μm
Peak wavelength	1470 nm	1590 nm
FWHM	1.3 nm	1.2 nm
FSR	158.4 nm	141 nm
Finesse	121	117
Insertion loss	1.76 dB	1.59 dB

FWHM = full width at half maximum, FSR = free spectral range. FSR = free spectral range.

5. Discussion

5.1. Electromechanical design

The four sets of straight-beam suspensions of width w, length l, and height h have a total elastic rigidity of $k = 4 \times E(w^3h/l^3)$ for the lateral motion of the stage [17]. The suspension width designed to be 5 μm was measured to be 4 μm after microfabrication, mainly due to the side-etching of silicon DRIE step. Substituting $w = 4$ μm, $l = 250$ μm, and $h = 50$ μm, the rigidity is calculated to be $k = 131$ N/m. For N-pairs of comb-drive electrodes, we write the electrostatic attractive force as $F_E(V) = (1/2)\varepsilon_0(h/g)V^2 \times N$, where $g = 1.5$ μm is the lateral gap between comb fingers, $\varepsilon_0 = 8.85 \times 10^{-12}$ F/m the dielectric constant of vacuum, and V is the applied voltage. In this model, we neglected the attraction force acting on the comb tips. Equating the mechanical restoring force $k_v x$ with the electrostatic force $F_E(V)$, one could numerically solve the equation to find the displacement x–voltage V curve, as shown by the solid line in Fig. 6, which was in good agreement with the experimentally obtained data.

As shown in Figs. 6 and 7, typical drive voltage was as high as 60 V mainly due to the suspensions that were intentionally made stiff enough to support the reflector cube against the gravity. It could be designed to be lower to make the device acceptable for low-voltage driver electronics. Reducing the suspension rigidity would not be a good idea because the Fabry-Pérot performance becomes attitude-dependent but actuators of larger output force should be sought for.

From the dimension parameters used in the mask design, the mass of the movable stage was estimated to be $m_{stage} = 0.38$ mg. The resonant frequency before putting a reflector cube was thus calculated to be $f_0^{OFF} = 1/2\pi\sqrt{k/m_{stage}} = 2.95$ kHz. Adding a mass of the reflector cube ($m_{cube} = 2.65$ mg) would lower the resonant frequency to $f_0^{ON} = 1/2\pi\sqrt{k/(m_{stage} + m_{cube})} = 1.12$ kHz, which also agreed well with the experimentally observed resonance peak of 1 kHz.

5.2. Optical design

The q-th mode wavelength of the Fabry-Pérot resonance is written as $\lambda_q = 2d/q$, where d is the air gap between two parallel reflectors [11]. Free spectral range (FSR) between the q-th and $q+1$-th modes is written by the difference of the mode wavelengths as

$$\mathrm{FSR} = \lambda_q - \lambda_{q+1} = 2d\left(\frac{1}{q} - \frac{1}{q+1}\right).$$

Judging from the measured value of FSR = 141 nm and the measured air gap of $d = 6$ μm at 63.9 V, the mode number q is estimated to be an integer of 9. Using the peak wavelength of 1470 nm, the Fabry-Pérot gap is back-calculated to be $d = q\lambda_q/2 = 6.6$ μm; this value is consistent with the experimentally measured value of air gap shown in Fig. 6. For the same value of q, one would obtain the air-gap change $\Delta d = q/2(\lambda_q^H - \lambda_q^L)$, where λ_q^H and λ_q^L are the peak wavelengths under two different drive voltages. Using the wavelength values 1470 and 1590 nm in Table 1, theoretical change of the air gap is $\Delta d = 0.54$ μm, which is also supported by the experimentally obtained value of 0.6 μm.

6. Conclusions

Hybrid-assembly of reflector cubes on a MEMS actuator platform was found to be a promising technique to make a compact wavelength tunable filter. Wavelength range can be easily set by choosing appropriate sets of reflector cubes, without compromising device performance associated to the MEMS fabrication incompatibility such as intrinsic film stress or chemical intolerance to the sacrificial layer etching. Despite the small volume of the cube reflectors, hybrid-assembly was carried out without difficulty by using a chip-bonding tool. Parallelism of the mirror surfaces remains to be solved but our recent experimental results have shown improvement.

References

[1] L.Y. Lin, E.L. Goldstein, Opportunities and challenges for MEMS in lightwave communications, IEEE J. Select. Topics Quant. Elec. 8 (1) (2002) 163–172.

[2] J.E. Ford, J.A. Walker, D.S. Greywall, K.W. Goossen, Micromechanical fiber-optic attenuator with 3 mu-s response, J. Lightwave. Tech. 16 (9) (1998) 1663–1670.

[3] J.H. Correia, M. Bartek, R.F. Wolfenbuttel, Bulk-microimachined tunable Fabry-Pérot microinterferometer for the visible spectral range, Sens. Actuators 76 (1999) 191–196.

[4] A. Tixier, J.P. Gouy, Y. Mita, H. Toshiyoshi, H. Fujita, Microactuated slider-based tunable filters for optical fiber transmission, in: IEEE/LEOS International Conference on Optical MEMS (MOEMS 99), August 27–29, Mainz, Germany, 1999.

[5] An NEC Co. Japanese patent pending, P2003-101138A.

[6] M. Noro, K. Suzuki, N. Kishi, H. Hara, T. Watanabe, H. Iwaoka, CO_2/H_2O gas sensor using a tunable Fabry-Pérot filter with wide wavelength range, in: Proceedings of the International Conference on Micro Electro Mechanical Systems (MEMS 2003), Kyoto, Japan, January, 2003, pp. 319–322.

[7] D. Hohlfeld, H. Zappe, Micro-machined tunable optical filters with optimized band-pass spectrum, in: Proceedings of IEEE 12th International Conference on Solid State Sensors, Actuators and Microsystems (Transducers '03), Boston, US, June 8–12, 2003, pp. 1494–1497.

[8] M. Panitz, W. Benecke, Electrostatic actuated interference filters as optical switches for projection display applications, in: Proceedings of IEEE 12th International Conference on Solid State Sensors, Actuators and Microsystems (Transducers '03), Boston, US, June 8–12, 2003, pp. 580–582.

[9] R. Nakamura, A. Murata, C. Chong, K. Yano, S. Kamisuki, Highly wavelength-selective MEMS Fabry-Pérot tunable filter, in: IEEJ Proceedings of the 22nd Sensor Symposium, Tokyo, 2005, pp. 37–40.

[10] G.D. Cole, E.S. Bjorlin, Q. Chen, C.-Y. Chan, S. Wu, C.S. Wang, N.C. MacDonald, J.E. Bowers, MEMS-tunable vertical-cavity SOAs, IEEE. J. Quant. Elec. 41 (3) (2005) 390–407.

[11] T. Joseph, Verdeyen: Laser Electronics, third ed., Prentice Hall, New Jersey, 1995, pp. 144–147.

[12] R.S. Tucker, D.M. Baney, W.V. Sorin, C.A. Flory, Thermal noise and radiation pressure in MEMS Fabry-Pérot tunable filters and lasers, IEEE. J. Select. Topics Quant. Elec. 8 (1) (2002) 88–97.

[13] J.D. Grade, H. Jerman, T.W. Kenny, A large-deflection electrostatic actuator for optical switching applications, in: Technical Digest of Solid-State Sensor and Actuator Workshop (Hilton Head 2000), Hilton Head Island, SC, June 4–8, 2000, pp. 97–100.

[14] J.D. Grade, H. Jerman, T.W. Kenny, Design of large deflection electrostatic actuators, J. Microelectromech. Syst. 12 (3) (2003) 335–343.

[15] M. Uekawa, H. Sasaki, D. Shimura, K. Kotani, Y. Maeno, T. Takamori, Surface-mountable silicon microlens for low-cost laser modules, IEEE Photon. Tech. Lett. 15 (7) (2003) 945–947.
[16] Y. Petremand, W. Noell, P.-A. Clerc, A. Imhof, M. Epitaux, M. Verdiell, N. de Rooij, Novel 2D MEMS based optical beamsteerer, in: Proceedings of the IEEE/LEOS International Conference on Optical MEMS and Their Applications (Optical MEMS 2004), August 22–26, Takamatsu, Japan, 2004, pp. 58–59.
[17] S.P. Timoshenko, J.N. Goodier, Theory of Elasticity, third ed., McGraw-Hill, New York, 1987.

Biographies

Toshio Yamanoi received BS degree in optical engineering from Tokai University, Kanagawa, Japan, in March 2000 and joined Koshin Kogaku Co., Ltd. in April. He has been working for the research and development of wavelength tunable semiconductor lasers. Since April 2004 he has been engaged in a project on optical MEMS development in contract with the Institute of Industrial Science, The University of Tokyo. From April 2005 to present, he has been temporary transferred to the holding company, Yamaichi Electronics Co., Ltd.

Takashi Endo received BS degree in optical engineering from Tokai University, Kanagawa, Japan, in March 1988. He has been working for the research and development of wavelength tunable semiconductor laser and tunable optics in Koshin Kogaku Co., Ltd. since 1994.

Hiroshi Toshiyoshi received MEng and PhD degrees in electrical engineering from the University of Tokyo, Tokyo, Japan, in 1993 and 1996, respectively. Since April 2002, he has been an assistant professor with the Institute of Industrial Science (IIS), the University of Tokyo, Tokyo, Japan. From April 1999 to March 2001, he had been a visiting assistant professor at University of California, Los Angeles for his sabbatical years. He is currently a Co-Director of the first Japan-France international research collaboration LIMMS (Laboratories for Integrated Micro Mechatronic Systems) with IIS. He also conducts a 3-year project on optomechatronics at Kanagawa Academy of Science & Technology (KAST) since April 2005. His main research interest is optical and RF MEMS.